JMEPEG (2011) 20:1242–1246
DOI: 10.1007/s11665-010-9770-6

1059-9495/$19.00

Effect of Strain Rate on Cathodic Reaction During Stress Corrosion Cracking of X70 Pipeline Steel in a Near-Neutral pH Solution

Z.Y. Liu, X.G. Li, and Y.F. Cheng

(Submitted February 26, 2010; in revised form August 26, 2010)

The effect of strain rate on cathodic reactions of X70 pipeline steel during stress corrosion cracking in a near-neutral pH solution was investigated by electrochemical impedance spectroscope and potentiodynamic polarization curve measurements as well as slow strain rate tests. A local additional potential model was used to understand mechanistically the role of strain rate in electrochemical cathodic reaction. It was found that an application of elastic stress would not affect the electrochemical stable state of the steel specimen at a macroscopic scale. Under a weak cathodic polarization, the interfacial charge-transfer process occurring on steel contains both cathodic and anodic reactions. Since the anodic reaction process is still significant, localized dissolution could occur even at such a cathodic potential, resulting in generation of corrosion pits. These pits could be the start sites to initiate stress corrosion cracks. Strain rate affects the corrosion reaction, which is associated with the generation of dislocation emergence points and slip steps on the specimen surface, resulting in a negative local additional potential to enhance the cathodic reaction locally.

Keywords cathodic reaction, pipeline steel, strain rate, stress corrosion cracking

1. Introduction

It has been acknowledged (Ref 1, 2) that stress corrosion cracking (SCC) is a potential threat to the safe operation of high-pressure natural gas pipelines. The pipeline SCC, usually occurring below the yield strength of the steel and typically below the design stress (Ref 3, 4), is divided into two categories, i.e., high pH SCC (Ref 5-8) and near-neutral pH SCC (Ref 9-14). It has been well accepted (Ref 1) that the high pH SCC is attributed to anodic dissolution at the grain boundaries, and is always associated with a concentrated carbonate/bicarbonate environment with a pH of about 9.5. The near-neutral pH SCC, occurring in an anaerobic, dilute bicarbonate solution with a pH of 6-7.5, shows a transgranular, quasi-cleavage crack morphology with very little branching (Ref 11-17). It has been proposed (Ref 18-22) that hydrogen is involved in the near-neutral pH SCC, accompanying anodic dissolution of the steel. The effect of applied stress on pipeline SCC was investigated and found that stress would enhance local anodic dissolution of the steel at crack-tip, accelerating the crack propagation (Ref 23). Moreover, a hydrogen-charging could increase the anodic dissolution rate of the steel, contributing to a high crack propagation rate (Ref 24-27). There is thus a synergism of stress, hydrogen, and anodic dissolution at the crack tip of the steel. In Cheng's thermodynamic model (Ref 28), it was proposed that an accurate prediction of the growth rate of stress corrosion cracks in steel under near-neutral pH condition depends on determination of a stress-affecting factor, a hydrogen-affecting factor, and a synergistic affecting factor of hydrogen and stress on the anodic dissolution rate of the steel at the crack tip.

Strain rate has been acknowledged as a critical factor to affect SCC process (Ref 29-32). In a recent study, a local additional potential (LAP) model was developed to illustrate the critical role of strain rate in SCC of the steel (Ref 33). According to the LAP model, both density and mobility of the local active spots on the steel surface, i.e., dislocation emergence points and slip steps, increase linearly with strain rate. Generation of such active spots introduces an additional negative potential locally, affecting the local electrochemical reactions and, consequently, the susceptibility of the steel to SCC.

In this study, the effect of strain rate on electrochemical cathodic reactions during near-neutral pH SCC of a X70 pipeline steel was illustrated mechanistically by LAP model, and verified experimentally by various electrochemical measurements, including electrochemical impedance spectroscope (EIS) and potentiodynamic polarization curves. The implication on pipeline SCC was analyzed.

2. Experimental

2.1 Specimen and Solution

Specimens used in this study were cut from a hot-rolling X70 steel plate, with the chemical composition (wt.%): 0.065 C, 0.23 Si, 1.57 Mn, 0.056 Nb, 0.20 Ni, 0.18 Cr, 0.22 Cu,

Z.Y. Liu, Mechanical Engineering, University of Calgary, Calgary, Canada and Corrosion and Protection Center, University of Science and Technology Beijing, Beijing, China; **X.G. Li**, Corrosion and Protection Center, University of Science and Technology Beijing, Beijing, China; and **Y.F. Cheng**, Mechanical Engineering, University of Calgary, Calgary, Canada. Contact e-mail: fcheng@ucalgary.ca.

0.0020 S, 0.0019 P, and Fe balance. The specimen, designed and machined according to ASTM A370 (Ref 34), was under the tensile direction that was vertical to the rolling direction. The mechanical properties of the steel specimen contained yield strength (σ_{ys}) 472 MPa, ultimately tensile strength (σ_{uts}) 626 MPa, minimum elongation (δ_0) 18.5%, and reduction-in-area (RA) 59.5%. The specimen was ground sequentially to 800 grit emery papers, with the grounding direction parallel to the loading direction. The specimen was then coated by an epoxy manufactured by LECO, leaving a working area of 0.8 cm × 0.8 cm.

The test solution was a NS4 solution, containing $CaCl_2 \cdot 2H_2O$ 0.181 g/L, $MgSO_4 \cdot 7H_2O$ 0.131 g/L, KCl 0.122 g/L, and $NaHCO_3$ 0.483 g/L. The solution was made from analytic grade reagents and ultra-pure water (18 MΩ cm in resistivity). Before test, the solution was purged with 5% CO_2 balanced with N_2 for 1 h to achieve an anaerobic and near-neutral pH condition (pH of 6.3-6.5). The gas flow was maintained throughout the test.

All the tests were performed at ambient temperature (about 22 °C).

2.2 Electrochemical Measurements on the Tensile Steel Specimen

Electrochemical measurements were conducted on X70 steel specimen without and with loading through a Solartron 1280C electrochemical measurement system, where the steel specimen was used as working electrode, a saturated calomel electrode (SCE) as reference electrode, and a platinum plate as counter electrode. The tensile test was carried out using a Bose Materials Test System.

It was realized that the potentiodyanmic polarization measurement is a steady-state electrochemical technique. However, since the applied stress was in the elastic region, it was approximately assumed that the specimen was in a relatively stable state. Potentiodynamic polarization technique was thus applicable to study the effect of strain rate on the SCC susceptibility of X70 steel in this study. Moreover, it was demonstrated that the applied stress/strain rate would not alter significantly the electrochemical state of the steel specimen, as monitored by corrosion potential (E_{corr}).

When investigating the effect of strain rate, the specimen was stressed to the desired level, i.e., 95% of yield strength of the steel, and then strained at various strain rates. Before the electrochemical measurement, the stress applied on the specimen was increased from zero to the desired level. The test solution was then added in the cell, and electrochemical tests were performed. The E_{corr} was monitored during slow strain rate test for 20-30 min. The electrochemical measurements were not started until E_{corr} achieved an approximately steady value during tension. When the electrochemical measurement was conducted at an applied cathodic potential, the specimen was pre-polarized for 20 min before test.

The potential sweep rate during potentiodynamic polarization measurement was 1 mV/s, scanning from −0.8 to 0 V relative to E_{corr}. During EIS measurement, a disturbing signal of 10 mV was applied, with a measuring frequency range from 10000 to 0.01 Hz. Three specimens were used under each test condition to ensure the reproducibility of the results.

Each test was conducted three times, and the given data point was the average of the three tests. Thus, three specimens were used for each data point acquisition in this study.

3. Results

3.1 Corrosion Potential Measurements

Figure 1 shows the time dependence of E_{corr} of the steel specimen at an applied stress of $0.95\sigma_{ys}$ under various strain rates. It is seen that a change of strain rate over a wide range did not affect E_{corr}, which was stabilized at about −0.75 V(SCE). The measurement results showed that, under the applied stress, the alteration of strain rate would not affect the electrochemical stable state of the specimen. Therefore, the steady-state electrochemical techniques could be used to investigate the corrosion behavior of the steel specimen under various strain rates.

3.2 EIS Measurements in the Absence of Stress/Strain Rate

Figure 2 shows the Nyquist diagrams measured at various cathodic potentials without application of stress and strain rate. It is seen that there was one semicircle over the measuring frequency range at E_{corr}, −800 and −850 mV(SCE), and there were overlapped semicircles at potentials −900 and −950 mV(SCE). When the cathodic potential was further shifted negatively, two semicircles were observed in both the

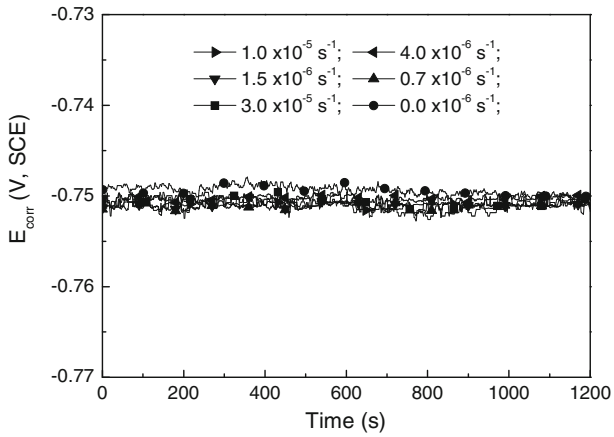

Fig. 1 Time dependence of corrosion potential of the steel specimen under various strain rates and an applied stress of $0.95\sigma_{ys}$

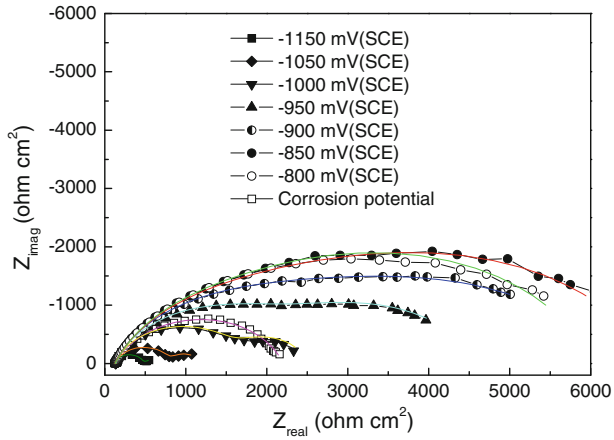

Fig. 2 Nyquist diagrams and the fitting curves measured on the steel specimen in the absence of stress and strain rate

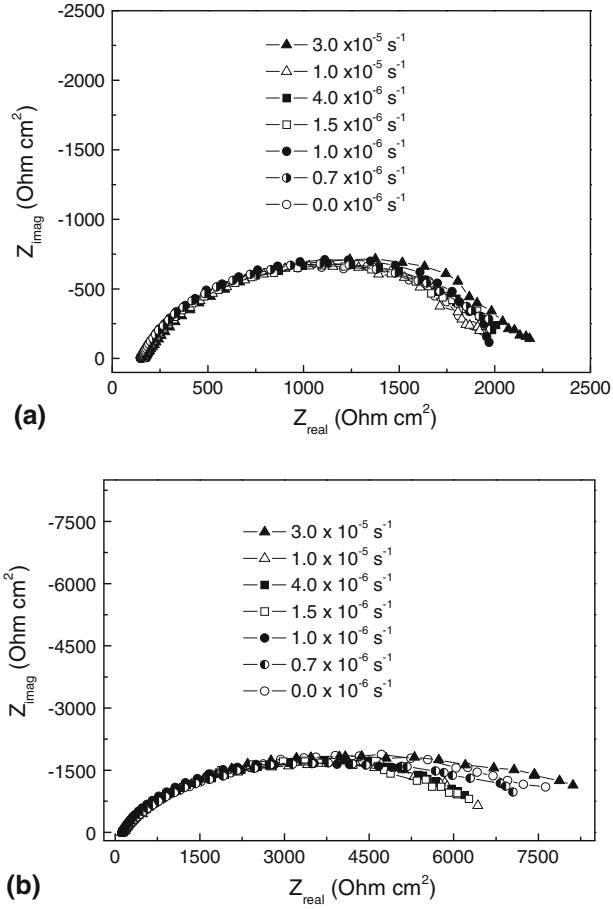

Fig. 3 Nyquist diagrams measured on the steel specimen at a stress of $0.95\sigma_{ys}$ under various strain rates at (a) corrosion potential, (b) −850 mV(SCE)

high- and low-frequency ranges. Furthermore, the size of the semicircle increased when the potential changed from E_{corr} to −850 mV(SCE), and then decreased with the negative shift of the cathodic potential.

3.3 Effect of Strain Rate on Electrochemical Measurements

Figure 3 shows the Nyquist diagrams measured on specimen at E_{corr} and −850 mV(SCE) under various strain rates. It is seen that there was a certain effect of strain rate, although slightly, on the measured EIS plots, and the effect became more apparent when the potential of the specimen was shifted from E_{corr} to −850 mV(SCE). The size of the impedance semicircles increased with strain rate when it was more than 5×10^{-6} s^{-1}. Since the semicircle size is associated with the charge-transfer resistance at the steel/solution interface, an increase of strain rate would enhance the resistance of the interfacial charge-transfer process.

The effect of strain rate on the cathodic polarization curve measured on the stressed steel specimen is shown in Fig. 4. In order to show the detail of the dependence of cathodic current density on strain rate, the cathodic current densities at individual potentials were re-plotted as a function of the logarithm of strain rate, as shown in Fig. 5. It is seen that the cathodic current density increased with strain rate. After attaining a maximum at a strain rate of approximately 5×10^{-6} s^{-1}, the cathodic current density decreased.

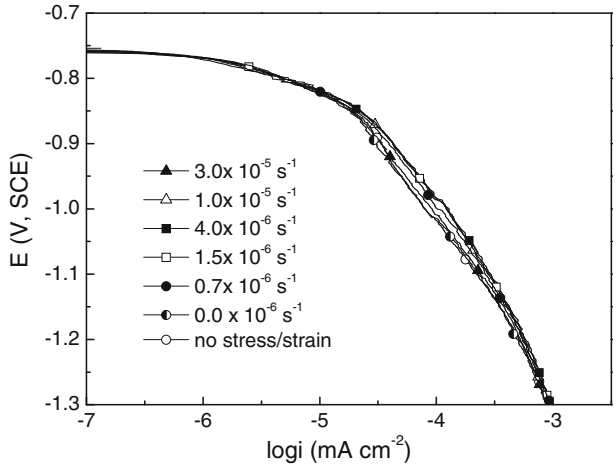

Fig. 4 Cathodic polarization curves measured on the steel specimen at a stress of $0.95\sigma_{ys}$ under various strain rates

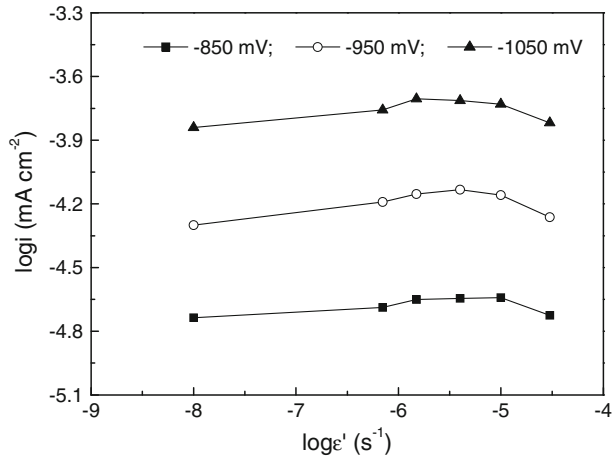

Fig. 5 Cathodic current density as a function of strain rate

4. Discussion

4.1 Potential Dependence of the Electrochemical Cathodic Reaction Mechanisms

The cathodic reactions occurring in the deoxygenated, near-neutral pH NS4 solution are primarily the reduction of bicarbonate ions and water (Ref 35):

$$HCO_3^- + e \rightarrow H + CO_3^{2-} \quad \text{(Eq 1)}$$

$$H_2O + e \rightarrow H + OH^- \quad \text{(Eq 2)}$$

The anodic reactions contain the oxidation of iron and the formation of a layer of iron hydroxide deposit (Ref 36):

$$Fe \rightarrow Fe^{2+} + 2e \quad \text{(Eq 3)}$$

$$Fe + 2H_2O \rightarrow Fe(OH)_2 + 2H^+ + 2e \quad \text{(Eq 4)}$$

Furthermore, a layer of iron carbonate scale would be formed on the electrode surface either electrochemically (Ref 37, 38)

$$Fe + HCO_3^- \rightarrow FeCO_3 + H^+ + 2e \quad \text{(Eq 5)}$$

or chemically:

$$Fe^{2+} + CO_3{}^{2-} \leftrightarrow FeCO_3 \quad \text{(Eq 6)}$$

Although the scale of $Fe(OH)_2$ and $FeCO_3$ provides a limited protection over the steel, electrochemical cathodic and anodic reactions still happen at the scale-free zone and even the holes/pores in the scale. When strain rate is introduced and a stress level is applied on the specimen, dislocation emergence points and slip steps would form on the specimen surface because of the dislocation movement, introducing a local additional negative potential to enhance the cathodic reactions locally. The coverage of the dislocation emergence points (DEP) on a unit surface, A_{DEP}, is (Ref 33):

$$A_{DEP} = \frac{n_0}{S/r_0^2} \times 100\% = \varepsilon' \times 100\% \quad \text{(Eq 7)}$$

where n_0 is the DEP density on the metal surface in unit time, S is the cross-sectional area normal to the tensile direction, r_0 is the atomic radius, and ε' is the applied strain rate. For a strain rate less than 3×10^{-5} s^{-1} in this study, A_{DEP} is not more than 0.003%. It is thus expected that the electrochemical surface state of the specimen would not be changed due to the generation of DEP. Therefore, an application of stress and strain rate would not shift the electrochemical state significantly, as demonstrated by the corrosion potential monitoring in Fig. 1.

When the steel specimen is under a weak cathodic polarization, such as from E_{corr} to −850 mV(SCE), the anodic partial reaction is still present (Ref 36, 37). Thus, the total charge-transfer impedance (R_{ct}^{T}) contains both anodic reaction impedance (R_{ct}^{a}) and cathodic impedance (R_{ct}^{c}):

$$\frac{1}{R_{ct}^{T}} = \frac{1-\theta_2}{R_{ct}^{a}} + \frac{\theta_2}{R_{ct}^{c}} \quad \text{(Eq 8)}$$

where θ_2 is the coverage of the zone for cathodic reactions, which increases with the negative shift of potential. While the anodic effect is not negligible, R_{ct}^{a} and θ_2 increase, and R_{ct}^{c} decrease as the potential shifts negatively, resulting in a decrease of $\frac{1-\theta_2}{R_{ct}^{a}}$ and an increase of $\frac{\theta_2}{R_{ct}^{c}}$. If $\frac{\partial\left(\frac{1-\theta_2}{R_{ct}^{a}}\right)}{\partial E} > \frac{\left|\partial\left(\frac{\theta_2}{R_{ct}^{c}}\right)\right|}{|\partial E|}$, according to Eq 8, R_{ct}^{T} increases since it is dominated by the factor $\frac{1-\theta_2}{R_{ct}^{a}}$. When $\frac{\partial\left(\frac{1-\theta_2}{R_{ct}^{a}}\right)}{\partial E} = \frac{\left|\partial\left(\frac{\theta_2}{R_{ct}^{c}}\right)\right|}{|\partial E|}$, R_{ct}^{T} reaches a maximum. With the further negative decrease of potential, the anodic reaction is inhibited completely, and R_{ct}^{T} is approximately equal to R_{ct}^{c}, which decreases continuously with the cathodic potential.

It is seen from the analysis that, from E_{corr} to −850 mV(SCE), the interfacial charge-transfer process contains both cathodic (reaction 1) and anodic (reactions 3-5) reactions. Since the anodic process is still important, the interfacial impedance would increase with the potential, as evidenced by the increase in the size of semicircle in this potential range in Fig. 2. The one semicircle is featured with the total charge-transfer reaction. With the negative shift of potential, the interfacial impedance achieves a maximum, and then decreases, as demonstrated in EIS plots in Fig. 2. The cathodic process is dominated by the hydrogen evolution (reaction 2).

It is worth pointing out that, for pipeline steel under a "weak" cathodic protection (CP) potential, the anodic reaction process is still significant. Localized dissolution could occur even at such a CP potential. It is actually a common phenomenon that corrosion pits are found on a pipeline steel under CP. These pits have been proposed to the start sites to initiate stress corrosion cracks. Therefore, a sufficiently negative CP potential must be applied on pipeline to avoid local anodic dissolution of the steel and the occurrence of corrosion pits.

4.2 Effect of Strain Rate on Electrochemical Reaction of the Steel

This study shows that strain rate affects the corrosion reaction significantly, as shown in Fig. 3-5. With the increase of strain rate, the number of dislocation emergence points on the specimen surface increases, resulting in a negative shift of LAP (Ref 33). As a result, the thermodynamics for cathodic reaction is favorable, and the cathodic current density increases, as seen in Fig. 5. When strain rate is up to 5×10^{-6} s^{-1}, a maximum of cathodic current density is observed. Below this value, the cathodic current density increases with strain rate, which is attributed to the favorable cathodic reaction due to the enhanced LAP effect. However, when strain rate is sufficiently high, such as 3×10^{-5} s^{-1}, the mobility of the dislocation emergence points is so fast that the reactive species do not have chance to adsorb at these active sites for reductive reaction. Thus, the cathodic current density decreases.

Furthermore, the dependence of cathodic current density on strain rate becomes less significant when the potential is shifted more negatively. When the cathodic potential is shifted negatively, such as to −1050 mV(SCE), all cathodic reactions proposed are thermodynamically feasible. The strain-induced LAP effect becomes less important compared to the negative potential of the steel specimen.

5. Conclusions

An application of stress in the elastic region would not affect the electrochemical stable state of the steel specimen at a macroscopic scale. The coverage of the dislocation emergence points, generated due to the applied stress/strain rate, on the specimen surface does not exceed 0.003%, and the electrochemical surface state would not change because of the generation of DEP.

For X70 steel in the near-neutral pH NS4 solution, from E_{corr} to −850 mV(SCE), the interfacial charge-transfer process contains both cathodic and anodic reactions. With the negative shift of potential, the interfacial impedance is dominated by cathodic reaction. For pipeline steel under a "weak" cathodic protection potential, the anodic reaction process is still significant. Localized dissolution could occur even at such a cathodic potential, resulting in generation of corrosion pits. These pits could be the start sites to initiate stress corrosion cracks.

Strain rate affects the corrosion reaction, which is associated with the generation of dislocation emergence points and slip steps on the specimen surface, resulting in a negative local additional potential. As a result, the thermodynamics for cathodic reaction is locally favorable. A maximum of cathodic current density is observed under a strain rate of 5×10^{-6} s^{-1}.

Acknowledgment

This study was supported by Canada Research Chairs Program.

References

1. M. Baker, Jr., *Stress Corrosion Cracking Studies*, Integrity Management Program DTRS56-02-D-70036, Department of Transportation, Office of Pipeline Safety, USA, 2004
2. R.N. Parkins, A Review of Stress Corrosion Cracking of High-Pressure Gas Pipelines, *Corrosion'2000*, NACE, Houston, 2000 (Paper No. 363)
3. E. Gamboa, V. Linton, and M. Law, Fatigue of Stress Corrosion Cracks in X65 Pipeline Steels, *Inter. J. Fatigue*, 2008, **30**, p 850–860
4. Z.Y. Liu, X.G. Li, C.W. Du, G.L. Zhai, and Y.F. Cheng, Stress Corrosion Cracking Behavior of X70 Pipe Steel in an Acidic Soil Environment, *Corros. Sci.*, 2008, **50**, p 2251–2257
5. A. Torres-Islas, J.G. Gonzalez-Rodriguez, J. Uruchurtu, and S. Serna, Stress Corrosion Cracking Study of Microalloyed Pipeline Steels in Dilute $NaHCO_3$ Solutions, *Corros. Sci.*, 2008, **50**, p 2831–2839
6. J.Q. Wang and A. Atrens, SCC Initiation for X65 Pipeline Steel in the "High" pH Carbonate/Bicarbonate Solution, *Corros. Sci.*, 2003, **45**, p 2199–2217
7. J.M. Sutcliffe, R.R. Fessler, W.K. Boyd, and R.N. Parkins, Stress Corrosion Cracking of Carbon Steel in Carbonate Solutions, *Corrosion*, 1972, **28**, p 313–338
8. M.C. Li and Y.F. Cheng, Corrosion of the Stressed Pipe Steel in Carbonate-Bicarbonate Solution Studied by Scanning Localized Electrochemical Impedance Spectroscopy, *Electrochim. Acta*, 2008, **53**, p 2831–2836
9. R.N. Parkins, W.K. Blanchard, Jr., and B.S. Delanty, Transgranular Stress Corrosion Cracking of High Pressure Pipelines in Contact with Solutions of Near Neutral pH, *Corrosion*, 1994, **50**, p 394–408
10. J. Sanchez, J. Fullea, C. Andrade, and C. Alonso, Stress Corrosion Cracking Mechanism of Prestressing Steels in Bicarbonate Solutions, *Corros. Sci.*, 2007, **49**, p 4069–4080
11. L. Niu and Y.F. Cheng, Corrosion Behavior of X-70 Pipe Steel in Near-Neutral pH Solution, *Appl. Surf. Sci.*, 2007, **253**, p 8626–8631
12. C.W. Du, X.G. Li, P. Liang, Z.Y. Liu, G.F. Jia, and Y.F. Cheng, Effects of Microstructure on Corrosion of X70 Pipe Steel in an Alkaline Soil, *J. Mater. Eng. Perform.*, 2009, **18**, p 216–220
13. G. van Boven, W. Chen, and R. Rogge, The Role of Residual Stress in Neutral pH Stress Corrosion Cracking of Pipeline Steels. Part I: Pitting and Cracking Occurrence, *Acta Mater.*, 2007, **55**, p 29–42
14. Y.F. Cheng and L. Niu, Mechanism for Hydrogen Evolution Reaction on Pipeline Steel in Near-Neutral pH Solution, *Electrochem. Commun.*, 2007, **9**, p 558–562
15. L. Zhang, X.G. Li, C.W. Du, and Y.F. Cheng, Corrosion and Stress Corrosion Cracking Behavior of X70 Pipeline Steel in a CO_2-Containing Solution, *J. Mater. Eng. Perform.*, 2009, **18**, p 319–323
16. M.P.H. Brongers, J.A. Beavers, C.E. Jaske, and B.S. Delanty, Effect of Hydrostatic Testing on Ductile Tearing of X-65 Line Pipe Steel with Stress Corrosion Cracks, *Corrosion*, 2000, **56**, p 1050–1058
17. J.G. Gonzalez-Rodriguez, M. Castles, V.M. Salinas-Bravo, J.L. Albarran, and L. Martinez, Effect of Microstructure on the Stress Corrosion Cracking of X-80 Pipeline Steel in Diluted Sodium Bicarbonate Solutions, *Corrosion*, 2002, **58**, p 584–590
18. B.Y. Fang, A. Atrens, J.Q. Wang, E.H. Han, and W. Ke, Review of Stress Corrosion Cracking of Pipeline Steels in "Low" and "High" pH Solutions, *J. Mater. Sci.*, 2003, **38**, p 127–132
19. B. Gu, J.L. Luo, and X. Mao, Transgranular Stress Corrosion of X80 and X52 Pipeline Steels in Dilute Aqueous Solution with Near Neutral pH, *Corrosion*, 1999, **55**, p 312–318
20. Y.F. Cheng, Analysis of Electrochemical Hydrogen Permeation Through X-65 Pipeline Steel and Its Implications on Pipeline Stress Corrosion Cracking, *Inter. J. Hydrogen Energy*, 2007, **32**, p 1269–1276
21. L.J. Qiao, J.L. Luo, and X. Mao, Hydrogen Evolution and Enrichment Around Stress Corrosion Crack Tips of Pipeline Steels in Dilute Bicarbonate Solution, *Corrosion*, 1998, **54**, p 115–120
22. Z.Y. Liu, G.L. Zhai, X.G. Li, and C.W. Du, Effect of Deteriorated Microstructures on Stress Corrosion Cracking of X70 Pipeline Steel in Acidic Soil Environment, *J. Univ. Sci. Technol. Beijing*, 2008, **15**, p 707–713
23. X. Tang and Y.F. Cheng, Micro-Electrochemical Characterization of the Effect of Applied Stress on Local Anodic Dissolution Behavior of Pipeline Steel Under Near-Neutral pH Condition, *Electrochim. Acta*, 2009, **54**, p 1499–1505
24. B. Gu, J.L. Luo, and X. Mao, Hydrogen-Facilitated Anodic Dissolution-type Stress Corrosion Cracking of Pipeline Steels in Near-Neutral pH Solution, *Corrosion*, 1999, **55**, p 96–106
25. M.C. Yan and Y.J. Weng, Study on Hydrogen Absorption of Pipeline Steel Under Cathodic Charging, *Corros. Sci.*, 2006, **48**, p 432–444
26. S. Dey, A.K. Mandhyan, S.K. Sondhi, and I. Chattoraj, Hydrogen Entry into Pipeline Steel Under Freely Corroding Conditions in Two Corroding Media, *Corros. Sci.*, 2006, **48**, p 2676–2688
27. M.C. Li and Y.F. Cheng, Mechanistic Investigation of Hydrogen-Enhanced Anodic Dissolution of X-70 Pipe Steel and Its Implication on Near-Neutral pH SCC of Pipelines, *Electrochim. Acta*, 2007, **52**, p 8111–8117
28. Y.F. Cheng, Thermodynamically Modeling the Interactions of Hydrogen, Stress and Anodic Dissolution at Crack-Tip During Near-Neutral pH SCC in Pipelines, *J. Mater. Sci.*, 2007, **42**, p 2701–2705
29. S.A. Serebrinsky, G.S. Duffó, and J.R. Galvele, Effect of Strain Rate on Stress Corrosion Crack Velocity: Difference Between Intergranular and Transgranular Cracking, *Corros. Sci.*, 1999, **41**, p 191–195
30. P.R. Rhodes, Environment-Assisted Cracking of Corrosion-Resistant Alloys in Oil and Gas Production Environments: A Review, *Corrosion*, 2001, **57**, p 923–966
31. N. Rokuro and M. Yasuaki, SCC Evaluation of Type 304 and 316 Austenitic Stainless Steels in Acidic Chloride Solutions Using the Slow Strain Rate Technique, *Corros. Sci.*, 2004, **46**, p 769–785
32. F.P. Ford, Quantitative Prediction of Environmentally Assisted Cracking, *Corrosion*, 1996, **52**, p 375–395
33. Z.Y. Liu, X.G. Li, C.W. Du, and Y.F. Cheng, Local Additional Potential Model for Effect of Strain Rate on SCC of Pipeline Steel in an Acidic Soil Solution, *Corros. Sci.*, 2009, **51**, p 2863–2871
34. ASTM A370-09ae1 Standard Test Methods and Definitions for Mechanical Testing of Steel Products
35. G.A. Zhang and Y.F. Cheng, On the Fundamentals of Electrochemical Corrosion of X65 Steel in CO_2-Containing Formation Water in the Presence of Acetic Acid in Petroleum Production, *Corros. Sci.*, 2009, **51**, p 87–94
36. G.A. Zhang and Y.F. Cheng, Micro-Electrochemical Characterization of Corrosion of Welded X70 Pipeline Steel in Near-Neutral pH Solution, *Corros. Sci.*, 2009, **51**, p 1714–1724
37. G.Z. Meng, C. Zhang, and Y.F. Cheng, Effects of Corrosion Product Deposit on the Subsequent Cathodic and Anodic Reactions of X70 Steel in Near-Neutral pH Solution, *Corros. Sci.*, 2008, **50**, p 3116–3122
38. A.Q. Fu, X. Tang, and Y.F. Cheng, Characterization of Corrosion of X70 Pipeline Steel in Thin Electrolyte Layer Under Disbonded Coating by Scanning Kelvin Probe, *Corros. Sci.*, 2009, **51**, p 186–190